applied optics

Apochromatic lens design in the short-wave infrared band using the Buchdahl dispersion model

Wei Wang,[1,2] Xing Zhong,[1,3,*] Jiang Liu,[3] and Xiaoheng Wang[1,2]

[1]Changchun Institute of Optics, Fine Mechanics and Physics, Chinese Academy of Sciences, Changchun, Jilin 130033, China
[2]University of Chinese Academy of Sciences, Beijing 100049, China
[3]Chang Guang Satellite Technology Co., Ltd., Changchun, Jilin 130102, China
*Corresponding author: hitsdww@163.com

Received 26 September 2018; revised 20 December 2018; accepted 20 December 2018; posted 20 December 2018 (Doc. ID 346848); published 25 January 2019

Chromatic aberration is an important artifact that influences image quality. Thus, it should be optimized during lens design. However, the typical combination and selection method of glass materials for the visible band can hardly satisfy the apochromatic requirements of short-wave infrared (SWIR) lenses. Therefore, we propose a method of glass selection for apochromatic lens design in the SWIR band through vector operation based on the Buchdahl model and third-order aberration theory. The proposed method overcomes limitations of traditional methods and unstable calculation results of special material properties. A design example is presented, which indicates that the proposed method can correct the secondary spectrum in the SWIR band and simplify the design using ordinary mass-produced glasses.

https://doi.org/10.1364/AO.58.000892

1. INTRODUCTION

The short-wave infrared (SWIR) has excellent optical properties and image quality and resolution comparable to those of visible (VIS) light. SWIR imaging technology can be employed in low-illumination backgrounds such as night illumination, and under harsh environments, such as mist and haze [1–3]. With the development of infrared focal plane arrays, SWIR imaging technology has been widely applied in high-resolution observation and machine vision.

For optical systems with such a wide waveband as SWIR, the secondary spectrum is the main obstacle in enhancing image quality. However, material selection is the key to correcting the secondary spectrum, and dispersion characteristics of materials vary greatly in SWIR. Consequently, the materials used for apochromatic lenses in the VIS band are unsuitable for apochromatic lenses in the SWIR band [1,4]. Thus, special materials are widely applied, but the unstable properties and poor availability of these materials complicate optical design [5–7].

The Buchdahl model provides a new material selection method. It is a polynomial model that describes the refractive index, and the theory derived from this model can be used for apochromatic lens design. Previous research on the Buchdahl model focused mainly on calculation of coefficients and fitting of the refractive index in VIS and near-infrared bands [8–10]. Considering the relationship of focal lengths between different wavelengths, Robb *et al.* [11,12] established a material selection method based on the Buchdahl model and used this model to correct the chromatic aberration of $n+1$ wavelengths in n different types of glasses for $n > 2$. Bráulio *et al.* [13] modified this method and applied it to practical optical design. The Buchdahl model was also applied to optical systems such as cemented doublet mirrors [14,15], triplets [15], and even microscope [16] and hyper refractive–diffractive [17] systems in thermal infrared. However, refractive index fitting and precision analysis have yet to be conducted in SWIR, and the Buchdahl model has yet to be applied for apochromatic lens design in SWIR.

Aiming to overcome the above problems, we introduced the Buchdahl model into SWIR and deduced a material selection method for apochromatic lens design in the form of vector operation. The proposed method can correct the secondary spectrum by using ordinary mass-produced optical glasses. The Buchdahl model was utilized to fit the refractive index in SWIR, and the fitting precision of materials from five manufacturers was analyzed. Then the material selection method was derived in detail based on third-order aberration theory. This selection method was subsequently demonstrated in a spatial coordinate system. Finally, a specific design example was given under the guidance of the Buchdahl model to verify the validity of the proposed method.

2. DISPERSION CHARACTERISTICS OF MATERIALS IN SWIR

Although the infrared focal plane arrays have been commercialized, the technology is still incomplete. Although SWIR covers a spectrum of 1–2.5 μm, the photon response range of most

SWIR detectors cannot reach this level. Widely used detectors are low-resolution ones with a large pixel size, and the classical photon response covers the range of 0.9–1.7 μm [1,3,18]. This type of detector was used in this study.

For an optical system composed of two materials with given focal length f', the secondary spectrum [19] is expressed as

$$\Delta l' = -f' \cdot \frac{P_1 - P_2}{V_1 - V_2}, \tag{1}$$

where V and P are the empirical formulas of the Abbe number and partial dispersion defined as

$$V = (n_{\text{central}} - 1)/(n_{\text{short}} - n_{\text{long}}),$$
$$P = (n_{\text{central}} - n_{\text{long}})/(n_{\text{short}} - n_{\text{long}}).$$

Equation (1) shows that materials with similar partial dispersion and a large difference between Abbe numbers are appropriate to correct the secondary spectrum [20–22]. Most optical glasses can be used in SWIR because of their excellent transmission, but the dispersion characteristics of these materials vary greatly in SWIR, as can be observed from the partial dispersion versus Abbe number graphs of different materials from Schott and CDGM catalogs shown in Fig. 1.

As shown in Fig. 1, almost all the materials are distributed in a narrow band, approximately forming a straight line in the VIS band. However, in SWIR, flint glasses with a high refractive index and large dispersion, such as SF66 and ZF12, approach the crown glasses with a low refractive index and small dispersion, which makes optical materials compressed into a mass. Abbe numbers should have a large difference for apochromatic lenses, and the Abbe numbers of the materials vary from 40 to 60 in SWIR, which is narrower than that (20 to 80) in the VIS band. This result indicates that the materials that can be selected for apochromatic lenses in SWIR are greatly reduced. With the change in dispersion characteristics, optical materials suitable for apochromatic lenses in the VIS band are no longer suitable for those in the SWIR band. Special optical materials, such as crystals, are widely applied in optical systems to satisfy the condition of apochromatic lens design. Although these crystals have excellent optical properties, their use gives rise to a series of new problems [23,24]. For instance, CaF_2 is an ideal crystal material for apochromatic lenses owing to its high transmission and unique partial dispersion characteristics [19,21]. However, it is very fragile, easy to deliquesce, and slightly soluble in water, which complicate its fabrication and the process of obtaining a large-scale lens blank. ZnSe and ZnS can also be utilized for apochromatic lenses, but these materials heavily depend on the fabrication method. For instance, using the gas phase method or sedimentation method considerably affects transmission [19,21]. Additional materials, such as SiO_2 and calcite, are unsuitable for making refractive optical elements because of the birefringence effect [19]. In summary, a method to select ordinary optical glasses for apochromatic lenses should be developed [25].

3. BUCHDAHL DISPERSION MODEL IN SWIR

A. Buchdahl Dispersion Model

Dispersion is a function of variation in the refractive index relative to the wavelength; accurately describing the refractive index is the precondition for further research. Many models describing the relationship of refractive index and wavelength have been proposed [11,19], among which the Schott model is the most widely adopted one by manufacturers:

$$N^2(\lambda) = A_0 + A_1\lambda^2 + \sum_{n=2}^{5} A_n\lambda^{2-2n}, \tag{2}$$

where $N(\lambda)$ represents the refractive index at wavelength λ, and A_i represent the coefficients of each material. Different models can be converted accurately using optical design software. Previous research [8,10] has shown that the refractive index fitting precision of the Schott model in the spectrum of 0.4–0.7 μm is about $\pm 3 \times 10^{-6}$, whereas that in the spectrum of 0.36–1.0 μm is about $\pm 5 \times 10^{-6}$. Although the fitting precision is slightly higher than $\pm 5 \times 10^{-6}$ outside the spectrum of 0.36–1.0 μm, it still satisfies the tolerance requirements.

According to the definition of dispersion, Eq. (2) can be expanded into the following form of Lagrange series:

$$\Delta N(\lambda) = a_0 + a_1\Delta\lambda + a_2(\Delta\lambda)^2 + a_3(\Delta\lambda)^3 + \cdots, \tag{3}$$

where $\Delta N(\lambda) = N(\lambda) - N(\lambda_0)$, $\Delta\lambda = \lambda - \lambda_0$, and λ_0 is the central wavelength. Unfortunately, Eq. (3) converges very slowly, and higher-order terms are needed to satisfy the convergence conditions, even $\Delta\lambda$ is very small [17]. The more rapidly

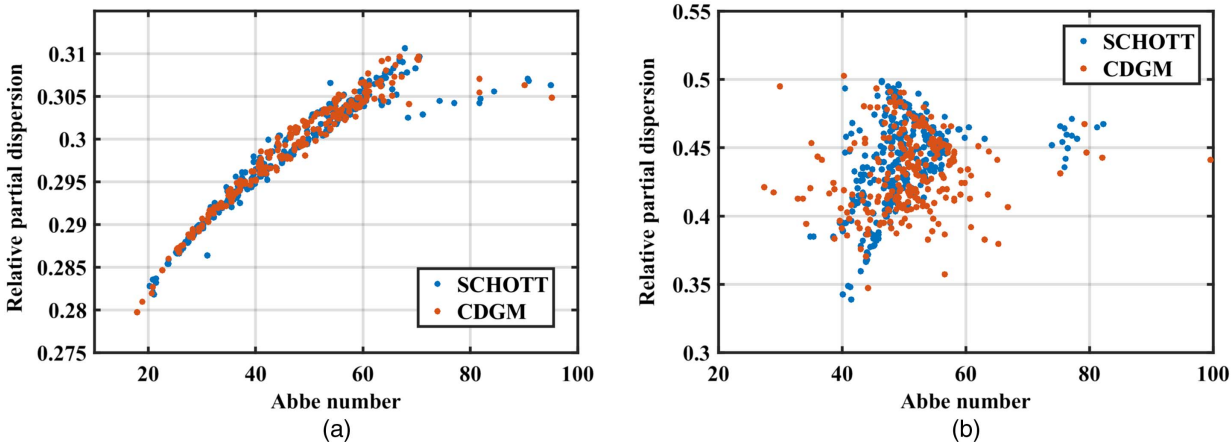

Fig. 1. Partial dispersion versus Abbe number in (a) visible band and (b) short-wave infrared band.

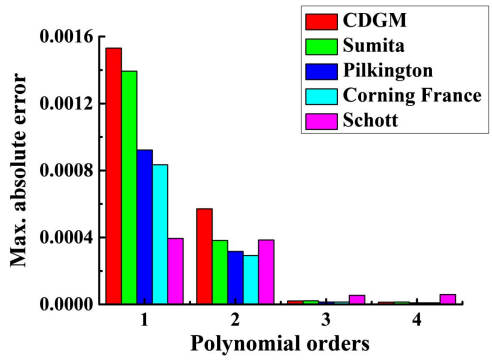

Fig. 2. Maximum absolute fitting error with different polynomial orders.

the polynomial converges, the simpler the aberration theory will be.

The Buchdahl model is a new fast-convergence refractive index model derived from the Hartmann model, which is still polynomial fitting of the refractive index and wavelength data [26]. Unlike other models, the Buchdahl model considers dispersion coordinate ω. The refractive index is converted from a function of wavelength into a function of dispersion coordinate. The Buchdahl model can be expressed as follows:

$$N = N_0 + \nu_1\omega + \nu_2\omega^2 + \nu_3\omega^3 + \cdots, \tag{4}$$

where N_0 is the refractive index at the central wavelength, and ν_i are the unique coefficients of each material.

When fitting the refractive index, reasonably choosing the order of polynomial can reduce calculation complexity while keeping the fitting precision [10]. For the spectrum of 0.4–0.7 μm, the square Buchdahl model can fit the refractive index very well, with a standard deviation of about 2×10^{-5} and maximum absolute errors of about 1×10^{-4}. For the spectrum of 0.365–1.014 μm, the cubic Buchdahl model performs very well, with a standard deviation of about 5×10^{-5} and a maximum absolute error of about 2.6×10^{-4}.

In order to determine the polynomial series suitable for the spectrum of 0.9–1.7 μm, we calculated the maximum absolute error of Buchdahl models with different orders for five glass catalogs. The calculation results are shown in Fig. 2. As the polynomial series changes from the first order to the third order, the maximum absolute error of each catalog decreases sharply. For higher orders after the third order, the change in the maximum absolute error becomes very slow, and the change is too small to be considered. Considering calculation complexity, here we choose the cubic Buchdahl model for the spectrum of 0.9–1.7 μm.

B. Dispersion Coordinate ω

Dispersion coordinate ω [26] is a function of wavelength expressed as follows:

$$\omega = \frac{\lambda - \lambda_0}{1 + \alpha(\lambda - \lambda_0)}, \tag{5}$$

where α is the scale factor, and its value depends on the operation wavelength ranges. The effect of scale factor α causes the Buchdahl model to converge rapidly, which straightens the refractive index curve in the coordinate system consisting of dispersion coordinate ω. Figure 3 displays the refractive index curves of BK7 in different coordinates. In the coordinates of wavelength λ, the curve shows the bending property. In the coordinates of dispersion coordinate ω, the curve is approximately linear with a certain slope.

According to the properties above, by fitting the refractive index curves of different α, we can choose the one that makes the curve close to a straight line as the optimal solution of α of each material. The calculation process is shown in Fig. 4. The refractive index curves of BK7 change continuously with the change in α, and the curve is close to a straight line when α is near 0.0612.

We calculated the scale factors of 1044 materials from five manufacturers, such as Schott and CDGM. Table 1 lists the range of α and maximum absolute error calculated in different catalogs. The column named Glass represents the glass corresponding to the maximum absolute error in each catalog. Aside from a few materials such as H-LAK59, the values of α of all the materials are distributed in a narrow range of 0–0.8. Thus, α can be regarded as a constant, which is similar to that in the VIS and near-infrared bands [10]. In this study, we take the mean value of α (0.4086) as the constant. Once α is determined, the coefficients ν_i can be accurately calculated.

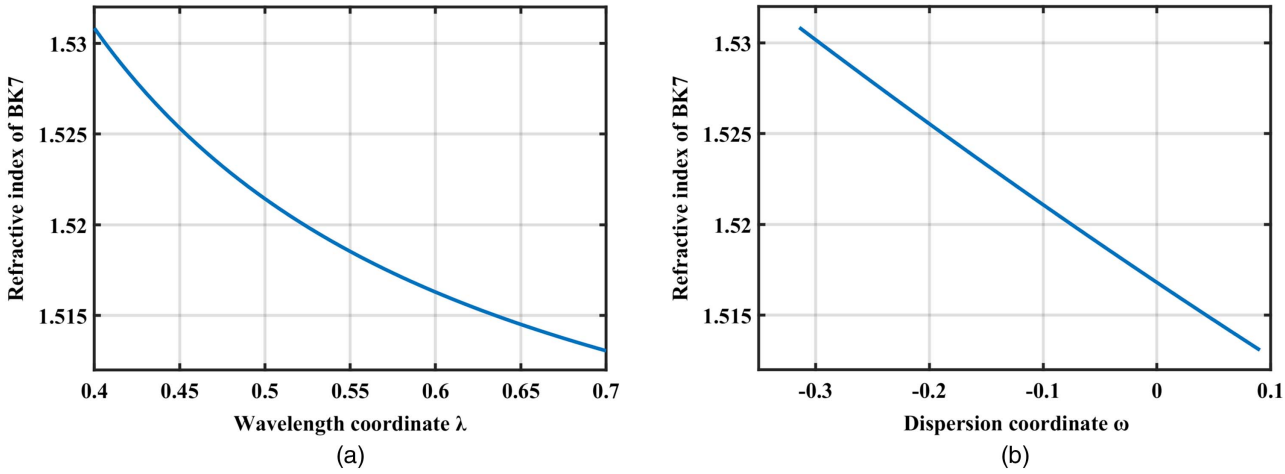

Fig. 3. Refractive index curves of BK7 under (a) wavelength coordinates and (b) dispersion coordinates.

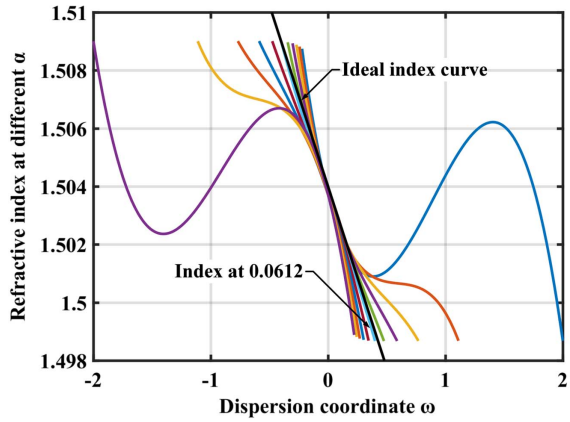

Fig. 4. Refractive index curves of BK7 with different ω values.

Table 1. Calculation of α with Different Manufacturers

Catalog	Range of α	Optimum α	Max. Error	Glass
Schott	0.0071–0.8058	0.325	6.2954×10^{-5}	N-KZFS2
CDGM	0.0253–0.7636	0.412	2.0915×10^{-5}	ZF52
Corning	0.0456–0.6535	0.411	1.4386×10^{-5}	E0525
SUMITA	0.0432–0.8049	0.462	3.6699×10^{-5}	KPSFN173
Pilkington	0.0145–0.9054	0.433	1.0729×10^{-4}	JLAK8

C. Calculation and Analysis of Buchdahl Model

Obtaining refractive index data is the premise of using the Buchdahl model, and the internal glass catalogs of Code V provide detailed refractive index data at specific wavelengths. In the process of precision analysis, we take the Schott model offered by Code V as the criterion. All the fitting results are compared with the data from the Schott model. The central wavelength is set to 1.3 μm in the spectrum of 0.9–1.7 μm.

In addition to the data at central and edge wavelengths, Code V provides refractive index data at 1.06 μm and 1.5296 μm. Using these five pairs of data, we can express Eq. (4) as the following matrix form:

$$\begin{bmatrix} \omega_1 & \omega_1^2 & \omega_1^3 \\ \omega_2 & \omega_2^2 & \omega_2^3 \\ \omega_3 & \omega_3^2 & \omega_3^3 \\ \omega_4 & \omega_4^2 & \omega_4^3 \\ \omega_5 & \omega_5^2 & \omega_5^3 \end{bmatrix} \begin{bmatrix} \nu_1 \\ \nu_2 \\ \nu_3 \end{bmatrix} = \begin{bmatrix} N_1 - N_0 \\ N_2 - N_0 \\ N_3 - N_0 \\ N_4 - N_0 \\ N_5 - N_0 \end{bmatrix}. \tag{6}$$

The least square method is an effective method for solving Eq. (6), in which the subscript of each parameter represents different wavelengths. Some of the fitting results are listed in Table 2. Figure 5 shows the fitting precision of materials from the two most used catalogs, Schott and CDGM. The envelope curves are the maximum and minimum statistical errors for the cubic Buchdahl model. The results demonstrate that the cubic Buchdahl model acts so well in the spectrum of 0.9–1.7 μm that the absolute fitting error of the Schott catalog is kept within 7×10^{-5}, whereas that of the CDGM catalog is kept within 2.5×10^{-5}, which completely satisfies the precision requirements of tolerance analysis. The fitting error curves converge at the central wavelength of 1.3 μm, which is consistent with theoretical analysis.

4. METHOD OF GLASS SELECTION FOR APOCHROMATIC

A. Dispersion Power

Dispersion is the first-order differential of refractive index with wavelength [19], and the refractive index is a continuous function of wavelength; thus, the dispersion should also be a continuous function of wavelength. Continuous dispersion is called instantaneous dispersion [27,28]. The relation of the Abbe number and instantaneous dispersion can be expressed as

$$V' = -\frac{1}{2}\frac{n(\lambda) - 1}{dn/d\lambda}. \tag{7}$$

Equation (7) is called the instantaneous Abbe number. By proper algebraic transformation, the Buchdahl model of Eq. (4) can be rewritten as follows:

$$D = \frac{\Delta N}{N_0 - 1} = \sum_{i=1}^{k} \frac{\nu_i}{N_0 - 1}\omega^i = \sum_{i=1}^{k} \eta_i \omega^i, \tag{8}$$

where $D(\lambda)$ is the dispersion power, k is the polynomial order of the Buchdahl model, and η_i are the primary, secondary, and tertiary dispersion coefficients. Equation (7) has a reciprocal relationship to Eq. (8) approximately, if we neglect the constant term and replace $dn/d\lambda$ with Δn when the wavelength approaches the central wavelength. In other words, dispersion power $D(\lambda)$ is the reciprocal of instantaneous Abbe number V', or Eq. (8) is the Lagrange polynomial expansion of the reciprocal of Eq. (7).

B. Method of Glass Selection

In the third-order aberration theory [19], the chromatic aberration of a thin lens is dependent on focal length and ray height, and the ray height is related to air space. A relationship of $-u'_k$ exists between axial chromatic aberration and lateral chromatic aberration. Thus, we analyze only lateral chromatic aberration in this study. The cemented thin lenses group is the simplest optical structure, whose thickness and air space can be considered zero.

Table 2. Calculation of Some Materials

Material	N_0	ν_1	ν_2	ν_3	Max. Error
CaF_2	1.42722	−0.004915	−0.000888	−0.002316	3.021204×10^{-6}
Silica	1.44714	−0.010405	−0.006511	−0.007111	5.397995×10^{-6}
H-FK61	1.48785	−0.007077	−0.001479	−0.003239	3.103174×10^{-6}
ZF12	1.72755	−0.021045	−0.002266	−0.012215	8.360192×10^{-6}
BK7	1.50372	−0.012059	−0.012059	−0.005197	3.307846×10^{-5}
N-SF66	1.87225	−0.027296	0.0030493	−0.014697	2.113214×10^{-5}

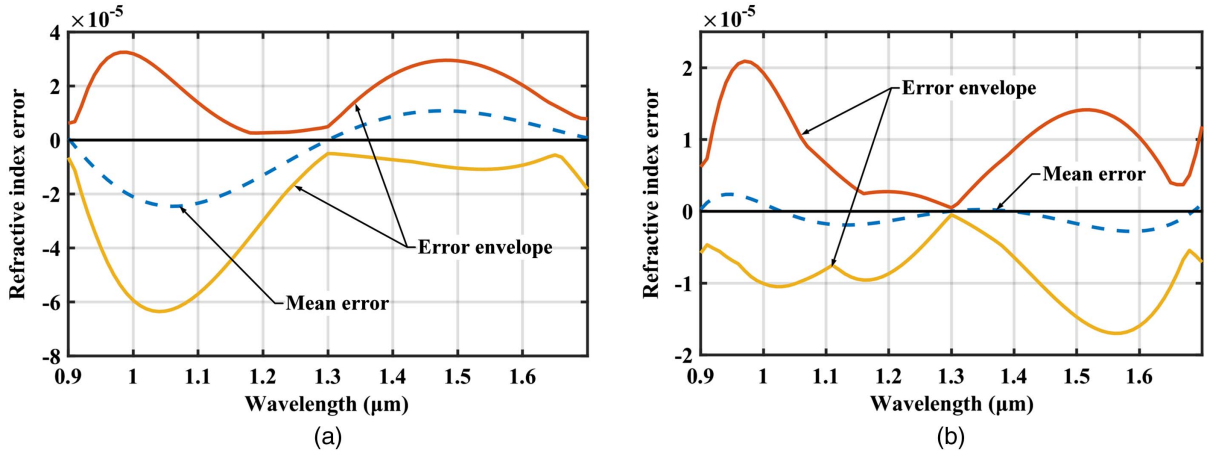

Fig. 5. Refractive index fitting error of (a) Schott catalog and (b) CDGM catalog.

Assuming a cemented thin lenses group with the stop aperture on the lens imaging for an object located at infinity, the lateral chromatic aberration [19] can be expressed as

$$\mathrm{TAchc} = \sum_{j=1}^{m} \frac{y_j^2 \phi_j}{u_k' V_j}, \tag{9}$$

where TAchc is the lateral chromatic aberration, y_j is the ray height of the j-th lens, ϕ_j is the focal power of the j-th lens, V_j is the Abbe number of the j-th lens, and u_k' is the angle after the ray passing through the last surface of the system. Assuming the incident ray height on the first surface is y_1, for a system with focal length f' and focal power ϕ_0, we can determine from the geometrical optics that $u_k' = -y_1/f' = -\phi_0 y_1$.

Assuming the Abbe number in Eq. (9) can be replaced by the instantaneous Abbe number, we can convert and express the lateral chromatic aberration as

$$\mathrm{TAchc} = -y_1 \sum_{j=1}^{m} \frac{y_j^2 \phi_j}{y_0^2 \phi_0} D_j(\lambda). \tag{10}$$

If we define $\alpha_j = y_j^2 \phi_j / y_1^2 \phi_0$, then Eq. (10) can be further written in the following form:

$$\mathrm{TAchc} = -y_1 \sum_{j=1}^{m} \alpha_j D_j(\lambda). \tag{11}$$

Taking the cubic Buchdahl model into Eq. (11), we can obtain the following equation:

$$\eta_{10}\omega + \eta_{20}\omega^2 + \eta_{30}\omega^3 = \sum_{j=1}^{m} [\alpha_j (\eta_{1j}\omega + \eta_{2j}\omega^2 + \eta_{3j}\omega^3)], \tag{12}$$

where η_{i0} is the sum of the i-th dispersion coefficients, and η_{ij} is the i-th dispersion coefficient of a specific lens represented by subscript j. For any given wavelength, ω is a constant; if we ignore ω, then Eq. (12) is not existent and divided into three equations as shown below:

$$\eta_{i0} = \sum_{j=1}^{m} \alpha_j \eta_{ij} \qquad (i = 1, 2, 3). \tag{13}$$

For an optical system described by Eq. (13), each glass material can be uniquely described by a coordinate point of $(\eta_{1j}, \eta_{2j}, \eta_{3j})$ in a 3D coordinate system consisting of dispersion coefficients.

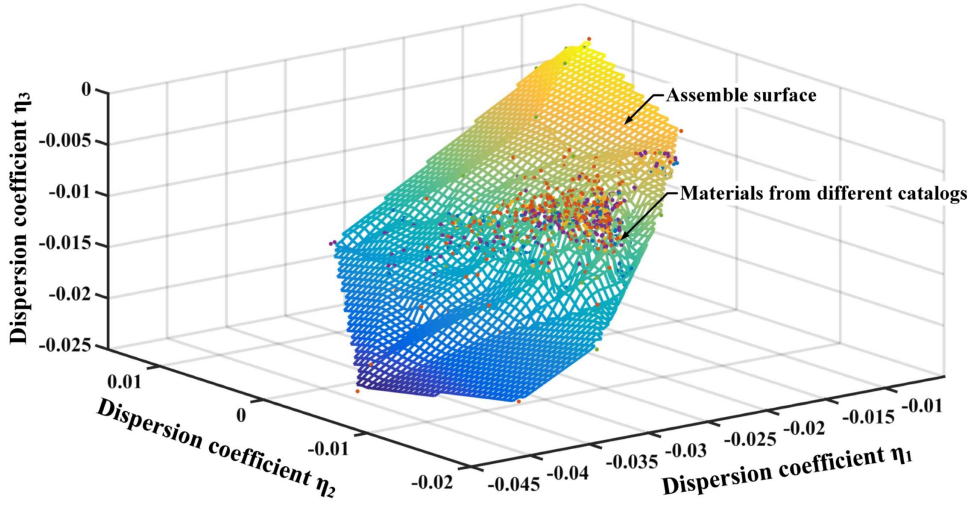

Fig. 6. Distribution of all materials in 3D coordinate system.

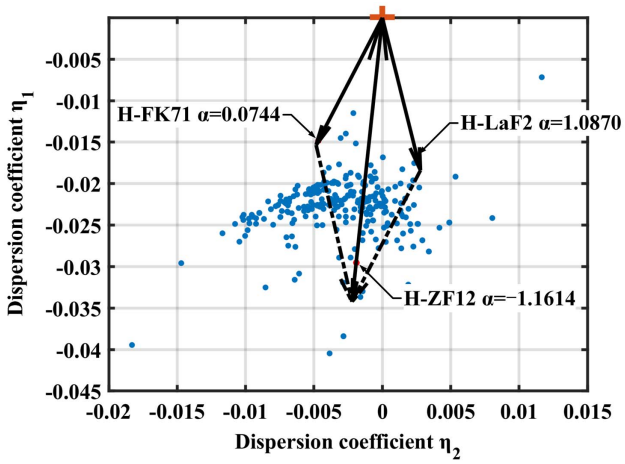

Fig. 7. Diagram of vector operation of three-material combination.

Table 3. Calculation of Three-Material Combinations

Glass Combination	α_1	α_2	α_3	Length
H-FK61/H-K3/ZF52	2.4302	−1.0651	−0.3650	7.7159×10^{-5}
H-FK61/H-F51/TF3	2.2424	−0.0992	−1.1432	9.0584×10^{-5}
H-FK61/H-K9L/ZF52	2.5610	−1.2000	−0.3636	3.2415×10^{-4}
H-FK61/H-F51/H-ZBaF1	2.7000	−0.3191	−1.3806	1.3640×10^{-4}
H-FK61/H-F51/H-ZK5	2.6977	−0.4493	−1.2485	8.6891×10^{-4}

By multiplying the point of $(\eta_{1j},\eta_{2j},\eta_{3j})$ with α_j, we can get a new coordinate point of $\alpha_j(\eta_{1j},\eta_{2j},\eta_{3j})$, where α_j corresponds to the scale factor. For a cemented thin lenses system under the normalized condition, the ray height on each lens is the same, which means α_j could be taken as the focal power of each lens. Thus the point of $\alpha_j(\eta_{1j},\eta_{2j},\eta_{3j})$ can be viewed as the dispersion effect caused by the selected glass.

The first-order dispersion (η_{10}) of the entire system can be viewed as the sum of the first-order dispersion coefficient of each glass. This relationship is also applicable to second-order and third-order dispersions. However, the overall dispersion is a combination of η_{10},η_{10}, and η_{10}. On this basis, if we take each glass as a vector in the 3D coordinate system, then an optical system can be made up of lenses in the form of a vector. By the method of vector operation, the whole dispersion of the system described as $(\eta_{10},\eta_{20},\eta_{30})$ can be calculated, which is the vector sum of each lens' dispersion:

$$\vec{G}_0=\sum_{j=1}^{m}\alpha_j\vec{G}_j,\qquad \vec{G}_j=\eta_{ij}\hat{x}+\eta_{2j}\hat{y}+\eta_{3j}\hat{z}. \tag{14}$$

$\vec{G}_0$ and $\vec{G}_j$ are space vectors in the 3D coordinate system, where $\vec{G}_0$ represents the dispersion vector of the whole system, $\vec{G}_j$ represents the dispersion vector of j-th glass, and $\hat{x}$, $\hat{y}$, and $\hat{z}$ are unit vectors. To ensure that the selected glass combination is appropriate for apochromatic lenses, we take the length of the sum vector as the criterion. Theoretically, the smaller the length of vector $\vec{G}_0$, the better the apochromatic ability of optical systems. Thus, we can adjust the scale factors α_j of certain glasses to make the sum vector $\vec{G}_0$ close to zero.

We can visually demonstrate this process in the coordinate system. However, the vectors are difficult to display in 3D space. Fortunately, calculation results show that almost all materials, except for some such as silica, are distributed on one plane approximately (Fig. 6). The colorful points represent materials from different catalogs; these points are assembled together onto a surface similar to a plane. Based on this property, the 3D coordinate system can be projected onto a 2D coordinate system using high-dimensional projection. Selecting glass materials in 2D space using dispersion coefficients η_1 and η_2 is easier than that in 3D space [15].

C. Example of Apochromatic Design Using Three Materials

Combining three glass materials provides more controllable variables for optimal design without the need to match the focal powers strictly, which is helpful to correct primary and residual aberrations. Therefore, three glass materials are usually combined for apochromatic lenses. The vector equation of three glass materials for apochromatic lenses is written as

$$\alpha_1\vec{G}_1+\alpha_2\vec{G}_2+\alpha_3\vec{G}_3=0. \tag{15}$$

Figure 7 shows the process of selecting three materials using vector operation in the 2D projection coordinate system. H-FK71 and H-LaF2 form positive lenses because of the small positive focal powers, and H-ZF12 forms a negative lens due to

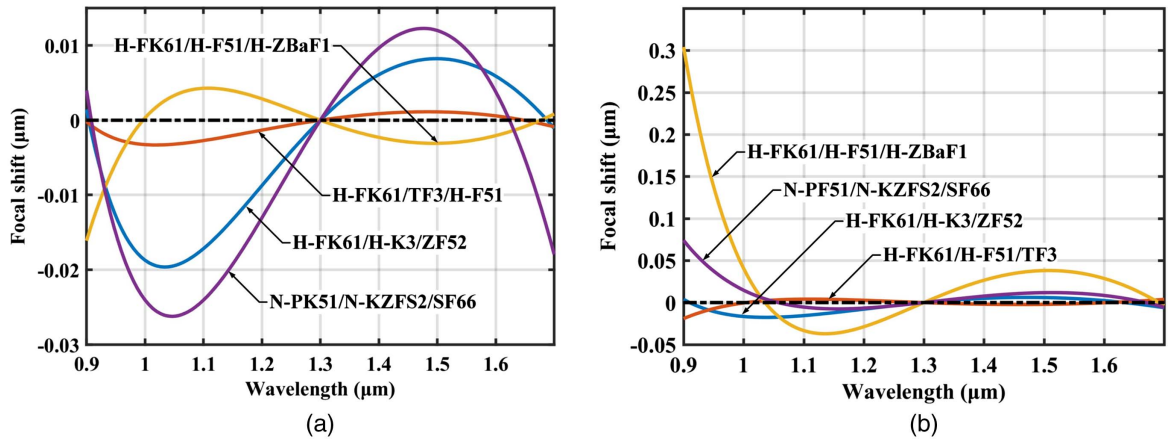

Fig. 8. Focal shift curves of systems designed by (a) new method and (b) traditional method.

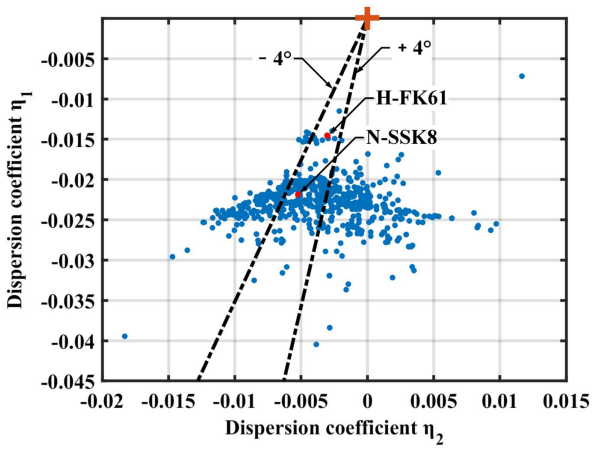

Fig. 9. Dispersion vector operation diagram of two-material combinations.

Table 4. Calculation of Several Two-Material Combinations

Glass Combination	α_1	α_2	Length
H-FK61/H-K12	3.0703	−2.0703	0.0014
H-FK61/TF3	2.3393	−1.3393	0.0015
H-FK61/H-F4	2.0265	−1.0265	0.0026
H-FK61/H-ZF3	1.7586	−0.7586	0.0034
H-FK61/ZF12	1.8282	−0.8282	0.0050

the large negative focal power. The sum of the focal powers equals one, and the sum vector is close to zero. Some calculation results of the normalized optical system are listed in Table 3.

The combinations listed in the table have great apochromatic ability. The only difference is that the wavelengths achieving apochromatic are inconsistent with the design wavelengths. Figure 8 shows the focal shift curves of different optical systems designed with the combinations listed in Table 3. These optical systems all have a unit focal length at F/4, imaging for objects at infinity. The initial target is correcting the secondary spectrum using central and edge wavelengths. As a comparison, the systems in Fig. 8(a) are designed by the new method proposed in this paper, and the systems in Fig. 8(b) are designed by the method discussed in section 2. Compared with the new method, the traditional method can also achieve apochromatic through simple optimization, but the performance is far inferior to the new method. The focal shift of the traditional method is obviously larger than that of the new method under the same conditions; the wavelengths used for apochromatic of the traditional method differ more greatly from the design wavelengths than that of the new method.

D. Example of Apochromatic Design Using Two Materials

Theoretically, the method shown in Fig. 7 is applicable no matter how many glasses are used. However, a special case would appear when selecting two materials, where the two materials selected need to be collinear with the original point [15]. Finding two materials that completely satisfy the requirements in 3D space is difficult, but Robb [11,12,15] reported that the perfect collinearity in applications is unnecessary. As shown in Fig. 9, if we take H-FK61 as a reference, the two-material combinations within the tolerance of about ±4 deg could be used for apochromatic lenses. Some calculation results of normalized optical systems are listed in Table 4, and Fig. 10 shows the focal shift curves similar to those in Fig. 8. Compared with Table 3 and Fig. 8, the apochromatic ability of two-material combinations is worse than that of three-material combinations. Optical systems in Fig. 10 have similar apochromatic ability, but the wavelengths used for apochromatic deviate significantly from the design wavelengths.

5. DESIGN EXAMPLE OF APOCHROMATIC SYSTEM

To verify the validity of the Buchdahl model, we designed an apochromatic camera based on the analysis above to correct the secondary spectrum at the pupil of 0.707 using wavelengths of 1.0 μm, 1.3 μm, and 1.7 μm. The design requirements are shown in Table 5.

A. Initial Structure of Optical System

To render the optical system lightweight and compact, we choose the telephoto objective lens as the initial model; all the surfaces are standard spheres [29]. The front group of

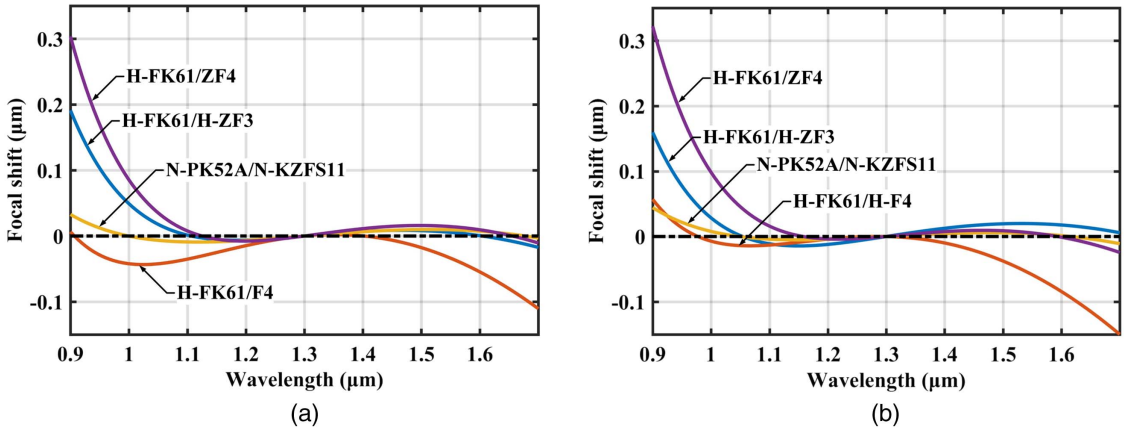

Fig. 10. Focal shift curves of systems designed by (a) new method and (b) traditional method.

Table 5. Design Requirements of Apochromatic Camera

Items	Requirements
Focal length	137.5 mm
Operating wavelength	1.0–1.7 μm
Relative aperture	1:4
Detector	640 × 512 pixels
Pixel size	25 × 25 μm

the system uses a triplet structure, which is used mainly to correct the secondary spectrum. The back group uses a doublet structure, which is used mainly to correct residual aberration. For the telephoto objective thin lens model with a focal length of 137.5 mm in this example, in order to balance the focal powers between the front and the back groups, here we make the total optical length of the system 0.8 of the focal length, and the distance between the front and back groups half of the total optical length. Therefore, the equivalent focal length of the front group is 91.67 mm, while it is −100 mm of the back group.

The selection of glasses is the key to correct the secondary spectrum. The FK glasses have the same optical properties as CaF_2, which renders it an ideal material for apochromatic lenses [19]. Lenses with a small radius of curvature are difficult to fabricate, whereas high-refractive-index materials can achieve a large radius of curvature. Thus, the dense flint glasses with a high refractive index can be used for apochromatic lenses. Referring to the analysis in section 4, the glasses used for the front group are ZF52, H-FK61, and H-K9L, while those used for the back group are H-FK61 and H-ZF3. All the glasses are frequently produced ones with high transmission and fine optical properties from the CDGM catalog.

The PWC method is a tool to determine the optical structure, whose parameters are functions of aperture angles, which are linked to the radius of curvature and glasses themselves. When using the PWC method, two special rays are usually introduced; one corresponds to the maximum field of view, and the other one passes through the edge of the stop aperture. The specific forms of primary aberrations can be determined by tracing the rays on each single surface, and then the initial structure can be solved. Figure 11 shows the ray tracing of a thin lenses system, and the thickness is just for display. The parameters marked with u and n are ray angles and refractive index, respectively, while those marked with h represent the ray height on each surface. Each parameter follows the symbolic rules defined in Ref. [19].

For a normalized thin lenses system, imaging for objects at infinity, assuming that the stop aperture is on the lens, then the incident angle $u = 0$, the marginal ray height $h = 1$, and the chief ray height $h_z = 0$. As shown in Eq. (16), only spherical aberration S_{I}, comatic aberration S_{II}, and longitudinal aberration C_{I} need to be solved for apochromatic lens design:

$$\begin{aligned}\sum S_{\mathrm{I}} &= \sum h^4\phi^3\overline{P} = \sum \overline{P},\\ \sum S_{\mathrm{II}} &= \sum h^3 h_z\phi^3\overline{P} + J\sum h^2\phi^2\overline{W} = J\sum \overline{W},\\ \sum C_{\mathrm{I}} &= h^2\phi\sum\frac{\phi}{\nu'} = \sum\frac{\phi}{\nu'},\end{aligned} \tag{16}$$

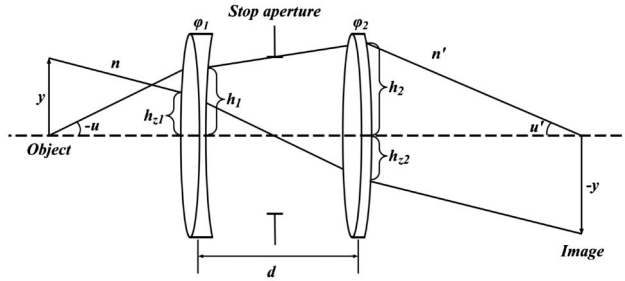

Fig. 11. Ray-tracing process of the thin lenses system.

where Abbe number ν is replaced by instantaneous Abbe number ν', and J is the Lagrange invariant. $\overline{P}$ and $\overline{W}$ are the normalized forms of P and W, defined as

$$\overline{P} = \frac{P}{(h\phi)^3} = \left(\frac{u'-u}{1/n'-1/n}\right)^2\cdot\left(\frac{u'}{n'}-\frac{u}{n}\right),$$
$$\overline{W} = \frac{W}{(h\phi)^2} = -\frac{u'-u}{1/n'-1/n}\cdot\left(\frac{u'}{n'}-\frac{u}{n}\right).$$

For the front group in this paper, by sorting out Eq. (16), we can get the relationship between the primary aberrations and the radius of curvatures. It is difficult to solve four unknown quantities (radius of curvature) using two equations (S_{I} and S_{II}), so here we introduce a new parameter, shape factor Q, to solve this problem. The shape factor is defined as $Q = 1/r_2 - \phi_1$, where r_2 is the radius of curvature of the second surface, and ϕ_1 is the focal power of the first lens. Using the focal power formulas of thin lenses, the radius of curvatures and Eq. (16) can be converted to a function of single unknown quantity Q finally. It is difficult to find a shape factor that satisfies both spherical aberration and comatic aberration, so the shape factor with smaller absolute value is usually adopted to generate large radius of curvatures. Here we take 2.7851 as the shape factor, and the aberrations of the front group are

$$\begin{aligned}S_{\mathrm{I\_front}} &= \sum\overline{P} = 1.6635,\\ S_{\mathrm{II\_front}} &= J\sum\overline{W} = -0.0137,\\ C_{\mathrm{I\_front}} &= \sum\frac{\phi}{\nu'} = -7.3124\times10^{-4}.\end{aligned}$$

The back group in this paper is used mainly to correct residual aberrations, which requires that the aberration of the back group and that of the front group compensate for each other as

$$\begin{aligned}S_{\mathrm{I\_front}} + S_{\mathrm{I\_back}} &= 0,\\ S_{\mathrm{II\_front}} + S_{\mathrm{II\_back}} &= 0,\\ C_{\mathrm{I\_front}} + C_{\mathrm{I\_back}} &= 0.\end{aligned}$$

Focal power distribution of the back group can be determined according to the principle of aberration compensation. Since the spherical aberration of the back group is always greater than zero, only the comatic aberration needs to be compensated. After calculation, we take −3.7398 as the shape factor, and the aberrations of the back group are

$$S_{\text{I\_back}} = \sum \overline{P} = 0.6221,$$
$$S_{\text{II\_back}} = J \sum \overline{W} = 0.0137,$$
$$C_{\text{I\_back}} = \sum \frac{\phi}{\nu'} = 7.3124 \times 10^{-4}.$$

According to the calculation result above, using the selected glasses and the allocated focal powers, the result of enlarging the initial structure calculated by the PWC method to the actual focal length is shown in Table 6.

B. Optimization of Optical System

The initial structure listed in Table 6 does not consider the thickness; thus, further optimization is needed. The first step of optimization is converting a thin lens into a thick lens by giving a certain thickness while maintaining focal power distribution.

The thickness of the lens is related not only to the radius of curvature and lens diameter, but also to the difficulty of processing and alignment. As a rule of thumb, central thickness, edge thickness, and external lens diameter satisfy the following mathematical relation:

$$d = x_1 + t - x_2, \qquad x_i = r_i \mp \sqrt{r_i^2 - (D/2)^2},$$

where x_i is the sagittal height of the lens, t is the edge thickness of the lens, and d is the central thickness of the lens. All parameters follow the symbolic rules defined in Ref. [19] . The Chinese standard GB/T 1205–1975 stipulates the minimum thickness of the center and edge of optical elements [30]. Using the above formula and the national standard, we can determine the thickness of each lens.

In this paper, the pupil diameter is 34.375 mm, and we give the lens a processing allowance of 2.5 mm considering the need of lens clamping. According to the national standard, for lenses with external diameters in the range of 30–50 mm, the minimum edge thickness of positive lenses is in the range of 1.8–2.4 mm, while the minimum central thickness of negative lenses is in the range of 2.2–3.5 mm. In order to reduce computational complexity and difficulty of lens processing and alignment, we set the central thickness of each lens to be greater than 4 mm, while the edge thickness is greater than 3 mm.

The focal power of a lens with a certain thickness is defined as

$$\phi = (n-1)\left[\left(\frac{1}{r_1} - \frac{1}{r_2}\right) + \frac{d(n-1)}{r_1 r_2 n}\right]. \tag{17}$$

Equation (17) shows that the focal power of the lens and the ray height on each surface change with the change in thickness. According to Eq. (10), the changes in ray height and focal power cause the change in lateral chromatic aberration; thus, these two parameters need to be controlled. It is quite complex and difficult to keep the ray height unchanged; however, the focal power can be easily kept unchanged as long as the radius of curvature of one surface changes. The radius of curvature can be calculated by using Eq. (17). For different types of lenses, the changing trend of the radius of curvature of the front surface and the back surface is different when the thickness increases, which is shown in Table 7.

In optical design, lenses with a large radius of curvature can reduce the advanced aberration and simplify the difficulty of lens processing. Therefore, according to Tables 6 and 7, for the lenses consisting of ZF52 and H-ZF3, we choose the front surface of each lens to adjust the radius of curvature, while we choose the back surface of the lens consisting of H-K9L to adjust the radius of curvature. For the convex and concave lenses consisting of H-FK61, we choose the front surface and the back surface to adjust the radius of curvature, respectively.

Based on the above analysis, we can convert the thin lens into the thick lens while maintaining focal power distribution. The thickness added to each lens and the structure of the initial system are listed in Table 8. ϕ_0 is the focal power of the lens in the actual optical system with a focal length of 137.5 mm, and r' is the adjusted radius of curvature of each lens. d_{center} and d_{rim} represent the central thickness and edge thickness, respectively. The thickness and focal power of the second lens in the front group are too large to improve transmission, which is not conducive to lightweight design or residual aberration correction. Therefore, it is necessary to separate this lens to disperse the focal power and enlarge the radius of curvature.

Once the thickness is determined, the distance between the front and back groups also changes correspondingly. The sum of the central thickness of all lenses and the distance between the front and back groups equals the distance between the front and back groups in the thin lens system. According to Table 8, the total thickness of the system is 28 mm, so the distance between the front and back groups should be 27 mm.

So far, we have formally established a thickness lens structure for further optimization. For those systems with special

Table 6. Initial Structure Calculated by PWC Method

Glass	ZF52	H-FK61	H-K9L	H-FK61	H-ZF3
n_0	1.8059	1.4878	1.5038	1.4878	1.6863
ϕ_0 (norm)	−0.3636	2.5610	−1.2000	1.8285	−0.8285
r_1	46.52	37.86	−32.41	−49.89	47.96
r_2	37.86	−32.41	−206.96	47.96	130.20

Table 7. Changing Trend of Curvature Radius

Lens	Front Surface	Back Surface
$r_1 > 0$ $r_2 < 0$	Reduce↓	Reduce↓
$r_1 < 0$ $r_2 > 0$	Rise↑	Rise↑
$r_1 > 0$ $r_2 > 0$	Rise↑	Reduce↓
$r_1 < 0$ $r_2 < 0$	Reduce↓	Rise↑

Table 8. Initial Structure of the Adjusted Thickness Lens

Glass	ZF52	H-FK61	H-K9L	H-FK61	H-ZF3
n_0	1.8059	1.4878	1.5038	1.4878	1.6863
ϕ_0	−0.003967	0.027938	−0.013091	−0.016623	0.007532
r_1'/mm	48.71	33.46	−32.41	−49.89	48.63
r_2'/mm	37.86	−32.41	−215.4909	49.22	130.20
d_{center}/mm	4	11.5	4	4	4.5
d_{rim}/mm	4.5	3.2	7.8	7.4	3.4

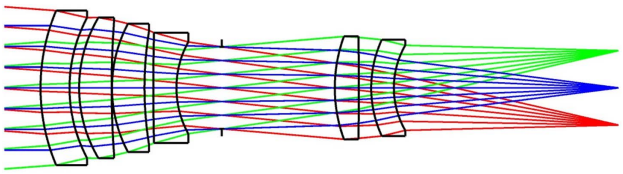

Fig. 12. Final optimized structure of the apochromatic camera.

requirements (such as apochromatic systems), it is easy to get a good initial structure by converting the thin lens into a thick lens, and the thickness of the lens should be optimized as a variable in the subsequent optimization process. Therefore, it is not necessary to give a very accurate solution of thickness in the conversion process.

The lenses of the initial structure can be separated appropriately to increase controllable variables and enhance the ability of correcting aberrations. The position of the stop aperture significantly influences lens size, field curvature, and distortion. Thus, we need to adjust the position of the stop aperture. In the optimization process, we should use the operands and constraints provided by optical design software such as ZEMAX or Code V to constrain the geometric and optical features of the system and meanwhile correct the aberration.

C. Final Optical System Structure

After iterative optimization, the final structure is shown in Fig. 12. The stop aperture is placed in the middle to balance the aberrations of the front group and back group. The lens composed of H-FK61 in the front group is separated into two lenses. The doublet structure of the back group is separated to correct field curvature, and the meniscus back toward the stop aperture corrects mainly astigmatism. The final system has good image quality, as shown in Fig. 13. The spot size of different fields of view on the image surface is distributed within the range of the Airy disk, and the modulation transfer function (MTF) within the Nyquist frequency of 20 lp/mm is close to the diffraction limit.

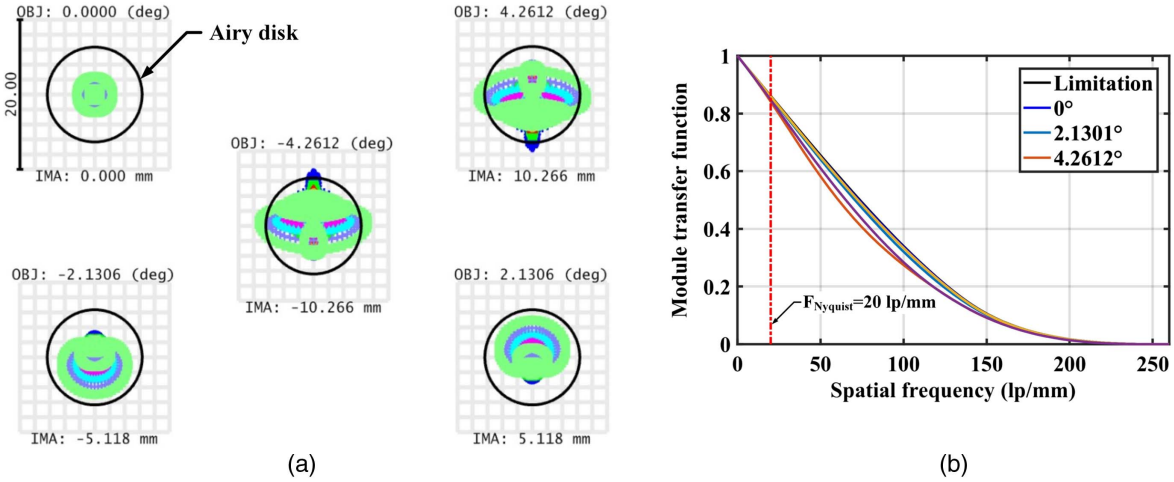

Fig. 13. Image quality graphs of the (a) RMS spot and (b) MTF.

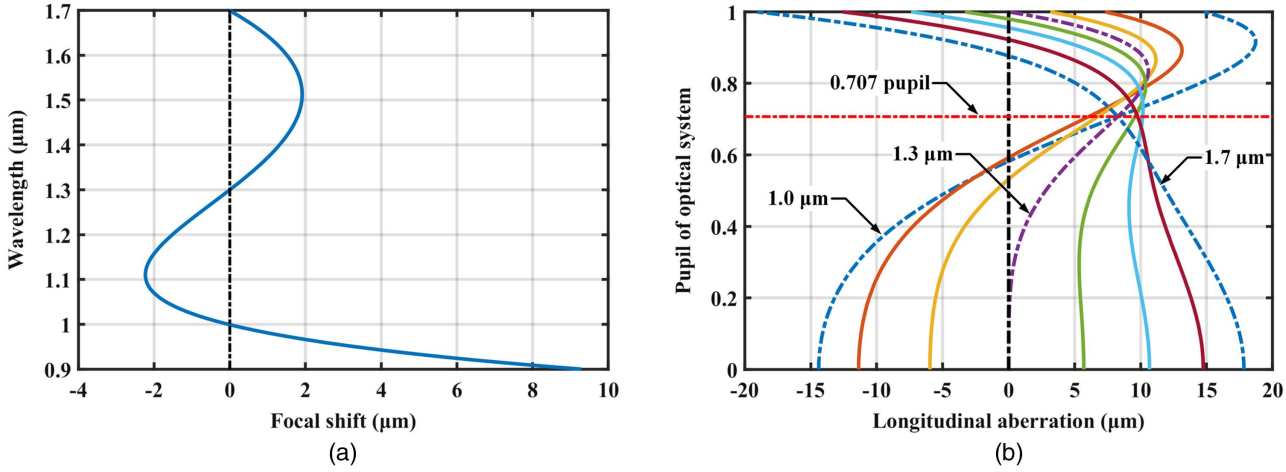

Fig. 14. Apochromatic results of (a) focal shift curve and (b) longitudinal aberration curves.

Table 9. Tolerance Allocation of the Final System

Items	Value
Surface irregular/λ	0.2–0.5
Radius/mm	0.1–0.15
Thickness/mm	0.01–0.02
Decenter/mm	0.01–0.02
Tilt	30”–50”
Refractive index	3×10^{-4}a€ 5×10^{-4}
Abbe number	0.5%–1.0%

According to the analysis above and Eq. (13), the total dispersion coefficients of the final optical system are

$$\eta_{10} = \sum_{j=1}^{6} \alpha_j \eta_{1j} = 2.313596 \times 10^{-4},$$

$$\eta_{20} = \sum_{j=1}^{6} \alpha_j \eta_{2j} = 7.415788 \times 10^{-5},$$

$$\eta_{30} = \sum_{j=1}^{6} \alpha_j \eta_{3j} = 1.196397 \times 10^{-4}. \quad (18)$$

The dispersion coefficients of the final system are quite small, which indicates that the system has good apochromatic ability. The apochromatic effect is illustrated in Fig. 14. For an apochromatic system, the focal length of each wavelength used to correct the secondary spectrum is the same; in other words, the focal shifts of these wavelengths are equal. In the figure of focal shift curve, the points at the wavelengths of 1.0 μm, 1.3 μm, and 1.7 μm coincide with zero. In the figure of the longitudinal aberration curves, the wavelengths of 1.0 μm, 1.3 μm, and 1.7 μm marked by dotted lines intersect in one point at the pupil of 0.707.

Tolerance analysis is used to estimate the quality of optical design, which is related to the capacity of fabrication and alignment. We take the average diffraction MTF at 20 lp/mm as the evaluation criterion and the back focal length as the compensation in the process of tolerance analysis. The tolerance allocation is listed in Table 9.

Tolerance analysis usually begins with a relatively loose tolerance and then adjusts the tolerance according to the analysis results until we find a tolerance that guarantees image quality and is not overly strict [16]. The tolerance analysis result is shown in Fig. 15 with reasonable tolerance allocation; the average MTF at 20 lp/mm is maintained over 0.6 with high probability, which means the final system compiles with the requirements of fabrication and alignment. The system is sensitive to the radius of curvature. Thus, the tolerance of the radius of curvature should be rigorously controlled.

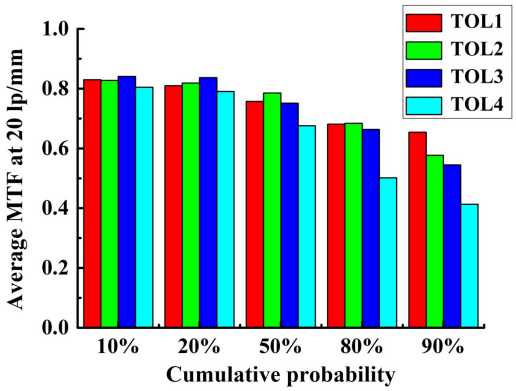

Fig. 15. Analysis results under different tolerance allocations.

6. CONCLUSION

We deduced a method of glass selection for apochromatic lens design based on the Buchdahl model and third-order aberration theory. This method of glass selection performed in the form of vector operation in a coordinate system consisted of dispersion coefficients. Theoretically, this method allows the system to correct the secondary spectrum in SWIR with ordinary mass-produced glasses combinations, whose properties are more reliable than those of special materials, such as crystals, while the dispersion characteristics and transmissions are comparable to those of special materials. Using the visualized spatial coordinate, once the glasses are selected, the dispersion characteristics of the system can be judged according to the length of the sum vector, which greatly simplifies the difficulty of apochromatic lens design. The new method avoids the unfavorable influences caused by using special materials, which reduces the difficulty of apochromatic lens design and consequently improves cost performance. To verify the validity of the new proposed method, we calculated the dispersion coefficients of 1044 materials and selected four ordinary glasses for specific apochromatic design. The design completely meets the requirements of fabrication, and the aberrations are well corrected. Depending on the comparison of the proposed method and the empirical method, this new proposed method overcomes the theoretical limitations of the traditional empirical formulas, and the apochromatic ability of the new proposed method is better than that of the traditional method to some extent. For glass selection and apochromatic lens design in other wavebands, this method offers instructional significance to some extent.

Acknowledgment. We sincerely thank the Optical Design Laboratory of Chang Guang Satellite Technology Co., Ltd., for its generous support during the period of this study.

REFERENCES

1. Y. Zhao, D. J. L. Williams, P. McCarthy, A. J. Visconti, J. L. Bentley, and D. T. Moore, “Chromatic correction for a VIS-SWIR zoom lens using optical glasses,” Proc. SPIE **9580**, 95800E (2015).
2. S. Bayya, D. Gibson, V. Nguyen, J. Sanghera, and G. Lindberg, “Design and fabrication of multispectral optics using expanded glass map,” Proc. SPIE **9451**, 94511N (2015).
3. R. H. Shepard and S. W. Sparrold, “Material selection for color correction in the short-wave infrared,” Proc. SPIE **7060**, 70600E (2008).
4. P. Hartmann, “Optical glass: dispersion in the near infrared,” Proc. SPIE **8167**, 816702 (2011).
5. J. Mao, M. Xu, Q. Liu, and W. Shen, “Design of refractive fore-optics with wide field of view and waveband for miniature imaging spectrometer,” Proc. SPIE **10021**, 100211S (2016).
6. M. P. Snyder and J. N. Vizgaitis, “Optical design study for the 1–5 μm spectral band,” Proc. SPIE **7298**, 729810 (2009).

7. L. A. Ryder, "Lens design for the near infrared camera for the James Webb space telescope," Proc. SPIE **5904**, 590409 (2005).
8. P. J. Reardon and R. A. Chipman, "Buchdahl's glass dispersion coefficients calculated from Schott equation constants," Appl. Opt. **28**, 3520–3523 (1989).
9. R. A. Chipman and P. J. Reardon, "Buchdahl's glass dispersion coefficients calculated in the near infrared," Appl. Opt. **28**, 694–698 (1989).
10. P. N. Robb and R. I. Mercado, "Calculation of refractive indices using Buchdahl's chromatic coordinate," Appl. Opt. **22**, 1198–1215 (1983).
11. P. N. Robb, "Selection of optical glasses," in *International LENS Design Conference* (1986), pp. 60.
12. P. N. Robb, "Selection of optical glasses. 1: two materials," Appl. Opt. **24**, 1864–1877 (1985).
13. C. D. A. B. Fonseca, J. Sasian, L. D. S. Fabiano, and A. S. Montes, "Method of glass selection for color correction in optical system design," Opt. Express **20**, 13592–13611 (2012).
14. N. V. Lessing, "Selection of optical glasses for cemented doublet mangin mirrors," Appl. Opt. **8**, 1245–1247 (1969).
15. R. D. Sigler, "Glass selection for airspaced apochromats using the Buchdahl dispersion equation," Appl. Opt. **25**, 4311–4320 (1986).
16. X. Jin-lai, G. Yan, and L. I. Dian-Meng, "Optical design of the N.A.0.75 plan-apochromatic microscope objective," Chin. J. Opt. **8**, 957–963 (2015).
17. Y. Pi, P. J. Reardon, and D. B. Pollock, "Applying the Buchdahl dispersion model to infrared hybrid refractive-diffractive achromats," Proc. SPIE **6206**, 62062O (2006).
18. M. Gerken and M. Münzberg, "Shortwave infrared camera with extended spectral sensitivity," Proc. SPIE **8353**, 835304 (2012).
19. W. J. Smith, *Modern Optical Engineering*, 4th ed. (2007).
20. D. Ren and J. R. Allingtonsmith, "Apochromatic lenses for near-infrared astronomical instruments," Opt. Eng. **38**, 537–542 (1999).
21. M. C. Gardner, P. J. Rogers, M. F. Wilde, T. Cook, and A. Shipton, "Challenges and solutions for high performance SWIR lens design," Proc. SPIE **9987**, 99870C (2016).
22. A. Mikš and J. Novák, "Method for primary design of superachromats," Appl. Opt. **52**, 6868–6876 (2013).
23. A. Yang, X. Gao, and M. Li, "Design of apochromatic lens with large field and high definition for machine vision," Appl. Opt. **55**, 5977–5985 (2016).
24. R. Duplov, "Apochromatic telescope without anomalous dispersion glasses," Appl. Opt. **45**, 5164–5167 (2006).
25. A. P. Grammatin and E. A. Tsyganok, "Apochromatic systems made from glasses with ordinary dispersion behavior," J. Opt. Technol. **79**, 202–204 (2012).
26. H. A. Buchdahl, *Optical Aberration Coefficients* (1954).
27. N. Carlie, "Broadband infrared optical materials and methods," in *International Optical Design Conference* (2014).
28. J. L. Ramsey and B. L. Unger, "Design of multiband optics using updated athermal/achromatic glass map," Proc. SPIE **10181**, 1018103 (2017).
29. M. Laikin, "*Lens Design*," 4th ed. (CRC Press, 2006).
30. "Minimum thicknesses in rim and center of lens," Report GB/T 1205-1975, (China State Administration for Market Regulation, 1975).